Letter

Hidden orders and (anti-)magnetoelectric effects in Cr_2O_3 and α-Fe_2O_3

Xanthe H. Verbeek ,[*] Andrea Urru , and Nicola A. Spaldin
Materials Department, ETH Zürich, 8093 Zürich, Switzerland

(Received 24 March 2023; revised 4 July 2023; accepted 6 October 2023; published 3 November 2023)

We present *ab initio* calculations of hidden magnetoelectric multipolar order in Cr_2O_3 and its iron-based analog, α-Fe_2O_3. First, we discuss the connection between the order of such hidden multipoles and the linear magnetoelectric effect. Next we show the presence of hidden antiferroically ordered magnetoelectric multipoles in both the prototypical magnetoelectric material Cr_2O_3 and centrosymmetric α-Fe_2O_3, which has the same crystal structure as Cr_2O_3 but a different magnetic dipolar ordering. In turn, we predict antimagnetoelectric effects, in which local magnetic dipole moments are induced in opposite directions under the application of an uniform external electric field to create an additional antiferromagnetic ordering. We confirm the predicted induced moments using first-principles calculations. Our results demonstrate the existence of hidden magnetoelectric multipoles leading to local linear magnetoelectric responses even in centrosymmetric magnetic materials, where a net bulk linear magnetoelectric effect is forbidden by symmetry, and broaden the definition of magnetoelectric materials by including those showing such local magnetoelectric responses.

DOI: 10.1103/PhysRevResearch.5.L042018

In 1936, Néel proposed a *hidden order* of antiparallel magnetic moments to explain the anomalous spike in the specific heat and magnetic susceptibility as a function of temperature in MnO [1]. Since then, many more hidden orders have been proposed, although they are usually either electric or magnetic in nature, among which we mention the antiferroic order of electric quadrupoles in UPd_3 [2] and the ferroic order of magnetic octupoles linked to the anomalous Hall effect in Mn_3Sn [3]. In this work, we show how magnetoelectric (ME) materials provide a platform for investigating a coupled magnetic-electric hidden order.

By definition, ME materials show a net change in magnetization M when an external electric field $\mathcal{E}$ is applied or vice versa change their electric polarization P in the presence of a magnetic field $\mathcal{H}$ [4]. These materials have been a subject of active research [5–7] as the coupling of magnetic and electric degrees of freedom is potentially useful for applications including low-energy-consumption memory devices, sensors, and transistors [8,9]. The lowest-order, *linear*, contribution to the ME response [10], which requires the simultaneous breaking of space- and time-inversion symmetries, is linked to the presence of ME multipoles [11–15], which are odd-parity, second-order multipoles of the magnetization density $\boldsymbol{\mu}(\boldsymbol{r})$. In their irreducible spherical form, the ME multipoles are the scalar ME monopole (a), the ME toroidal moment vector ($\boldsymbol{t}$) and the ME quadrupole tensor (q),

$$a = \frac{1}{3}\int \boldsymbol{r}\cdot\boldsymbol{\mu}(\boldsymbol{r})d^3\boldsymbol{r}, \tag{1}$$

$$t_i = \frac{1}{2}\int [\boldsymbol{r}\times\boldsymbol{\mu}(\boldsymbol{r})]_i d^3\boldsymbol{r}, \tag{2}$$

$$q_{ij} = \frac{1}{2}\int \left[r_i\mu_j(\boldsymbol{r}) + r_j\mu_i(\boldsymbol{r}) - \frac{2}{3}\delta_{ij}\boldsymbol{r}\cdot\boldsymbol{\mu}(\boldsymbol{r})\right]d^3\boldsymbol{r}, \tag{3}$$

which correspond respectively to the trace, the antisymmetric part, and the symmetric traceless part of the ME multipole tensor $\mathcal{M}_{ij} = \int r_i\mu_j(\boldsymbol{r})d^3\boldsymbol{r}$ [15]. ME multipoles provide a handle for understanding and predicting the linear ME effect starting from the microscopic environment since they have a one-to-one link to the linear ME tensor α_{ij}, defined as $\alpha_{ij} = \mu_0\partial M_j/\partial\mathcal{E}_i|_{\mathcal{H}}$, with μ_0 the vacuum permeability. Specifically, monopoles a and $q_{x^2-y^2}$, q_{z^2} quadrupoles account for the diagonal isotropic and anisotropic linear ME effect, whereas the toroidal moments t_i and the q_{xy}, q_{xz}, and q_{yz} quadrupoles are linked to the off-diagonal antisymmetric and symmetric linear ME effect, respectively. Analogously, the second-order ME effect can be captured by the next-higher-order magnetic multipoles, the magnetic octupoles [16].

$\mathcal{M}_{ij}$ can be decomposed into a sum over products of the atomic positions and their magnetic dipole moments, capturing the asymmetry in the unit-cell magnetization due to the arrangement of the magnetic dipoles [15], and local atomic-site contributions, which describe asymmetries in the local spin densities around each ion [15]. Here we focus on the local atomic-site multipoles, which occur in both ME and non-ME materials whenever the local Wyckoff site symmetry lacks both time reversal and space inversion. In centrosymmetric magnetic materials, where a net ME effect is forbidden by global inversion symmetry, these local multipoles are

[*]xverbeek@ethz.ch

Published by the American Physical Society under the terms of the Creative Commons Attribution 4.0 International license. Further distribution of this work must maintain attribution to the author(s) and the published article's title, journal citation, and DOI.

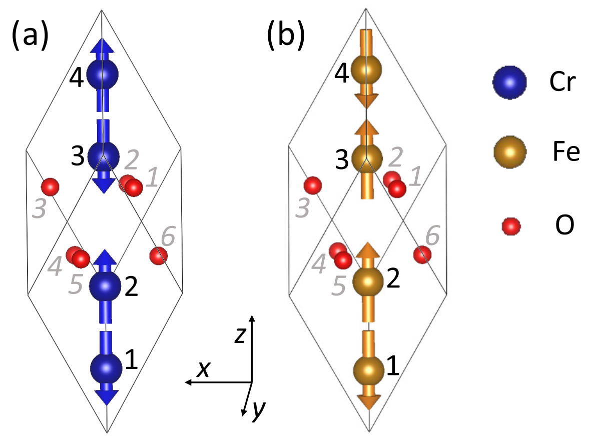

FIG. 1. Crystal structure and magnetic order of (a) Cr_2O_3 and (b) Fe_2O_3. Magnetic moments are indicated by arrows. The atoms are numbered following the conventional order of the Wyckoff positions. The magnetic easy axis is parallel to z.

TABLE I. Symmetry-allowed magnetic moments and ME multipoles and their ordering on the TM ions in Cr_2O_3 and Fe_2O_3. Atoms are labeled as in Fig. 1.

	Cr_2O_3				Fe_2O_3			
	Cr_1	Cr_2	Cr_3	Cr_4	Fe_1	Fe_2	Fe_3	Fe_4
m_z	$-m_{Cr}$	m_{Cr}	$-m_{Cr}$	m_{Cr}	$-m_{Fe}$	m_{Fe}	m_{Fe}	$-m_{Fe}$
a	$-a_{Cr}$	$-a_{Cr}$	$-a_{Cr}$	$-a_{Cr}$	a_{Fe}	a_{Fe}	$-a_{Fe}$	$-a_{Fe}$
t_z	t_{Cr}	$-t_{Cr}$	$-t_{Cr}$	t_{Cr}	t_{Fe}	$-t_{Fe}$	t_{Fe}	$-t_{Fe}$
q_{z^2}	$-q_{Cr}$	$-q_{Cr}$	$-q_{Cr}$	$-q_{Cr}$	q_{Fe}	q_{Fe}	$-q_{Fe}$	$-q_{Fe}$

antiferroically ordered but can in principle provide a *local* ME response. Indeed, such local symmetries have recently been shown to be important in explaining hidden Rashba and Dresselhaus effects in centrosymmetric materials [17,18].

In this work, we analyze the link between the local multipolar order and the local, atomic ME response in the isostructural materials Cr_2O_3 and α-Fe_2O_3 (from now on Fe_2O_3). Both materials adopt the corundum structure, with the centrosymmetric point group $\bar{3}m$ (space group $R\bar{3}c$), and are easy-axis antiferromagnets, below 307 K [19,20] and 263 K [21–23], respectively. Importantly, however, they have different magnetic orderings, as shown in Fig. 1. Specifically, the magnetic order in Cr_2O_3 breaks both inversion and time-reversal symmetries [magnetic space group (MSG) $R\bar{3}'c'$], whereas in Fe_2O_3 it breaks time-reversal symmetry only (MSG $R\bar{3}c$). As a result, Cr_2O_3 is a well-known ME material [24–28], in which the linear ME effect was first identified [4,29], whereas Fe_2O_3 does not show a net linear ME effect, and instead its symmetry allows a nonrelativistic, altermagnetic spin splitting [30,31]. Despite the difference in global symmetry, the local site symmetries are similar in Cr_2O_3 and Fe_2O_3. Local atomic ME multipoles and, in turn, a local ME response are allowed in both compounds, since the *local* inversion symmetry is broken at the Cr, Fe, and O Wyckoff sites in both materials. Thus, we expect that locally some of the special physics seen in Cr_2O_3 may be preserved in Fe_2O_3. Indeed, our main finding is that Fe_2O_3 has a *hidden* antiferromultipolar order that leads to a local anti-ME response, with a strength that is comparable to that in ME Cr_2O_3.

We demonstrate the existence of the hidden ME multipoles and quantify the size of the ME responses using density-functional calculations [32]. We compute the spin contributions to the local diagonal and off-diagonal lattice-mediated ME response in the xy plane using the method described in Ref. [33], modified to extract the *local atomic* magnetic response. This approach does not require the application of an electric field. Instead, the local ME response is computed by freezing in the atomic displacement corresponding to the electric field strength, computed from a superposition of infrared-active phonon modes as explained in Ref. [33]. For details, see the Supplemental Material [34]. Our density-functional calculations are performed within the noncollinear local spin density approximation (LSDA) [35], with spin-orbit interaction and Hubbard U correction [36] included, as implemented in the plane-wave code VASP [37,38] and in the augmented-plane wave (APW) code ELK [39]. We use VASP to compute the equilibrium structure and forces, and we interface it with phonopy [40,41] to obtain the phonon eigenvectors and frequencies. We use ELK to calculate the angular parts of the local magnetic multipoles, by decomposing the density matrix into its irreducible spherical tensors and extracting the relevant components [42], and to compute the ME responses. Since the resulting changes in the local magnetic moments are small at relevant phonon amplitudes, extensive convergence tests are performed (see the Supplemental Material [34]).

As described above, the linear ME effect requires time-reversal and inversion symmetries to be broken. This is the case in Cr_2O_3, but in Fe_2O_3 the global inversion symmetry is preserved. We determine which multipoles are allowed and their subsequent arrangement by studying both how each multipole transforms and how the atoms permute under the 12 symmetry operations of the $R\bar{3}c$ space group (for more details see the Supplemental Material [34]). We find that on the transition metal (TM) ions in Cr_2O_3 and Fe_2O_3, which have the same Wyckoff site symmetry (3), ME monopoles a, t_z toroidal moments, and q_{z^2} quadrupoles are allowed, but with different ordering. We support the results of our symmetry analysis with first-principles calculations of the multipole components in Cr_2O_3 and Fe_2O_3 at their respective equilibrium structures. These calculations confirm the multipolar ordering obtained from the symmetry analysis and provide the magnitude and absolute sign of each multipole (Table I; the signs correspond to the antiferromagnetic domains shown in Fig. 1), whereas the symmetry analysis yields only the relative sign on the different sites. The sizes of our calculated angular parts of a, t_z, and q_{z^2} (3×10^{-3}, 2×10^{-5}, and 2×10^{-3} μ_B in Cr_2O_3 and 4×10^{-3}, 7×10^{-5}, and 4×10^{-3} μ_B in Fe_2O_3, respectively) are similar in both materials, approximately scaling with the size of the calculated dipole moments (2.6 μ_B and 4.1 μ_B for Cr and Fe, respectively). The ferroic ordering of a and q_{z^2} ($- - - -$ in both cases) in Cr_2O_3 is consistent with its established anisotropic linear diagonal ME effect. On the other hand, in Fe_2O_3 the antiferroic ordering of a and q_{z^2} ($+ + - -$ in both cases) suggests an antiferroic linear diagonal ME response, in which an external electric field induces magnetic

TABLE II. Symmetry-allowed magnetic moments and ME multipoles, and their ordering on the O atoms in Cr_2O_3 and Fe_2O_3. When the sign is different in the two materials, two signs are given, with the top (bottom) sign corresponding to Cr_2O_3 (Fe_2O_3). The magnitudes (in μ_B) of m and the angular parts of a, t, q_1, q_2, q_3 are 7×10^{-5}, 1×10^{-2}, 1×10^{-2}, 2×10^{-2}, 4×10^{-5}, 1×10^{-2} in Cr_2O_3 and 2×10^{-3}, 3×10^{-2}, 2×10^{-2}, 2×10^{-2}, 3×10^{-4}, 4×10^{-2} in Fe_2O_3, respectively. Atoms are labeled as in Fig. 1.

	O_1	O_2	O_3	O_4	O_5	O_6
m_x	m	$-\frac{1}{2}m$	$-\frac{1}{2}m$	$\mp m$	$\pm\frac{1}{2}m$	$\pm\frac{1}{2}m$
m_y	0	$\frac{\sqrt{3}}{2}m$	$-\frac{\sqrt{3}}{2}m$	0	$\mp\frac{\sqrt{3}}{2}m$	$\pm\frac{\sqrt{3}}{2}m$
a	$\mp a$	$\mp a$	$\mp a$	$-a$	$-a$	$-a$
t_x	$+t$	$-\frac{1}{2}t$	$-\frac{1}{2}t$	$\pm t$	$\mp\frac{1}{2}t$	$\mp\frac{1}{2}t$
t_y	0	$+\frac{\sqrt{3}}{2}t$	$-\frac{\sqrt{3}}{2}t$	0	$\pm\frac{\sqrt{3}}{2}t$	$\mp\frac{\sqrt{3}}{2}t$
q_{xy}	0	$\mp\frac{\sqrt{3}}{2}q_2$	$\pm\frac{\sqrt{3}}{2}q_2$	0	$-\frac{\sqrt{3}}{2}q_2$	$+\frac{\sqrt{3}}{2}q_2$
q_{xz}	0	$+\frac{\sqrt{3}}{2}q_1$	$-\frac{\sqrt{3}}{2}q_1$	0	$\pm\frac{\sqrt{3}}{2}q_1$	$\mp\frac{\sqrt{3}}{2}q_1$
q_{yz}	$-q_1$	$+\frac{1}{2}q_1$	$+\frac{1}{2}q_1$	$\mp q_1$	$\pm\frac{1}{2}q_1$	$\pm\frac{1}{2}q_1$
$q_{x^2-y^2}$	$\pm q_2$	$\mp\frac{1}{2}q_2$	$\mp\frac{1}{2}q_2$	$+q_2$	$-\frac{1}{2}q_2$	$-\frac{1}{2}q_2$
q_{z^2}	$\mp q_3$	$\mp q_3$	$\mp q_3$	$-q_3$	$-q_3$	$-q_3$

moments parallel to the field but in opposite directions on Fe_1 and Fe_2 relative to Fe_3 and Fe_4, such that an antiferromagnetic order with no *net* magnetic moment is established along the field direction. We refer to this response as an *anti*-ME effect. Furthermore, the antiferroically ordered t_z in both materials, two orders of magnitude smaller than a and q_{z^2}, indicate an additional off-diagonal anti-ME effect, with the induced magnetic moments ordered differently in Cr_2O_3 (Cr_1 and Cr_4 having opposite sign relative to Cr_2 and Cr_3) and Fe_2O_3 (Fe_1 and Fe_3 having opposite sign relative to Fe_2 and Fe_4).

We note that in both materials local ME multipoles are allowed on the oxygen sites as well (Table II), where the absolute signs are obtained from our first-principles calculations. The Wyckoff site symmetry (2) of the O atoms does not include the threefold axis and thus allows multipoles with nonzero in-plane components (t_x, t_y, q_{xz}, q_{yz}, q_{xy}, and $q_{x^2-y^2}$), in addition to the a and q_{z^2} also found on the TM ions, while it prohibits t_z. Of all the multipole components on the O atoms, the only ones ordered ferroically are a and q_{z^2} in Cr_2O_3, indicating that the O atoms also contribute to the net ME effect in this material. All the other components sum to zero, as dictated by the global symmetry, and hence they do not contribute to a net ME effect but rather to additional anti-ME responses.

In addition to the ME multipoles associated with the linear ME effect, magnetic octupoles are also symmetry allowed. The relevant nonzero components on the TM ions are $\mathcal{O}_{-3}$ and $\mathcal{O}_3$, following the naming convention of Ref. [16] and, for an applied electric field along y, are associated with a local quadratic response in m_y and m_x, respectively [16,43]. $\mathcal{O}_3$ and $\mathcal{O}_{-3}$ are ordered antiferroically ($--++$ and $-+-+$, respectively) in Cr_2O_3, and correspond to a second-order diagonal and off-diagonal anti-ME effect [16]. In Fe_2O_3, $\mathcal{O}_{-3}$ orders antiferroically ($-++-$) as well, but $\mathcal{O}_3$ orders

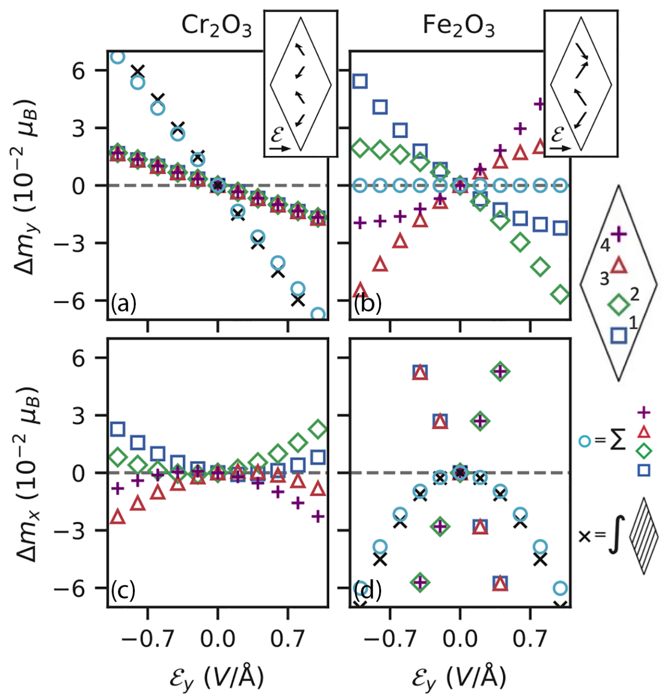

FIG. 2. Local change in the in-plane magnetic moments (Δm_i) on the TM ions as a function of the applied electric field strength, with Δm_i parallel [(a) and (b)] and perpendicular [(c) and (d)] to the applied electric field direction, in Cr_2O_3 [(a) and (c)] and Fe_2O_3 [(b) and (d)]. Blue squares, green diamonds, red triangles, and purple crosses represent Δm_i on TM ions 1–4, respectively. Cyan circles [(a), (b), and (d)] depict the sum of Δm_i on the four TM ions, and black diagonal crosses [(a) and (d)] show the total induced magnetic moments in the unit cell. Insets in (a) and (b) sketch qualitatively the linear response parallel to the applied $\mathcal{E}$, by showing the induced magnetic moments on top of the equilibrium magnetic order.

ferroically ($++++$), which suggests that the lowest-order *net* ME response is the second-order off-diagonal ME effect.

Now we use *ab initio* density-functional theory to calculate the anti-ME effects in Cr_2O_3 and Fe_2O_3 predicted by the symmetry arguments discussed above. Figure 2, which summarizes our results, shows the calculated lattice-mediated changes in the magnetic moments induced by an electric field pointing along the $+y$ direction for both Cr_2O_3 [Figs. 1(a) and 1(c)] and Fe_2O_3 [Figs. 1(b) and 1(d)], for the antiferromagnetic domains shown in Fig. 1. We separately consider the induced moments along y [Figs. 1(a) and 1(b)], associated with a diagonal ME response, and along x [Figs. 1(c) and 1(d)], associated with an in-plane off-diagonal response [44]. In Fig. 2(a), we see that the moments on all the four Cr atoms in Cr_2O_3 show an identical linear dependence on the strength of the applied electric field. This indicates an identical local diagonal linear ME response, adding up to a net diagonal linear ME effect over the unit cell. This is consistent with the ferroic ordering of a and q_{z^2} on the Cr ions. Furthermore, the sum of the induced local Cr magnetic moments (cyan circles) is close to the total induced magnetic moment per unit cell (black diagonal crosses), which includes contributions from the O atoms and the interstitial spaces, showing that the response is dominated by the Cr atoms.

TABLE III. Summary of the in-plane linear (L) and quadratic (Q) ME effects found in Cr_2O_3 and Fe_2O_3, classified as ferroic (F) and antiferroic (AF) responses.

	Diagonal		Off-diagonal	
	L	Q	L	Q
Cr_2O_3	F	AF	AF	AF
Fe_2O_3	AF	AF	AF	F

We remark that the sign of the response matches that found in previous first-principles calculations [33,45]. Although not visible in the plot, there is an additional small quadratic component to the induced magnetic moments as a function of electric field strength, but summed over the atoms this cancels out. This diagonal second-order anti-ME effect is consistent with the antiferroic ordering of the $\mathcal{O}_{-3}$ octupoles mentioned above.

The local induced magnetic moments parallel to the applied electric field on the four Fe atoms in Fe_2O_3 [Fig. 2(b)] show linear dependence for small field strengths, with identical magnitude, but order pairwise, with opposite sign for the two pairs of Fe ions, resulting in no net induced magnetic moment in the unit cell. This linear anti-ME effect, consistent with the antiferroic ordering of a and q_{z^2} discussed before, is the lowest-order ME response in Fe_2O_3 and, to the best of our knowledge, has not been previously discussed. In addition to the linear contribution, at high fields we note the presence of a non-negligible local quadratic response, consistent with the antiferroic ordering of the $\mathcal{O}_{-3}$ octupoles.

Next, we consider the induced in-plane magnetic moments perpendicular to the applied electric field, corresponding to the off-diagonal in-plane ME response. In Cr_2O_3 [Fig. 2(c)], these moments show a linear as well as a quadratic dependence on the strength of the applied electric field, but both contributions cancel out to make the net response zero. This indicates both a linear and quadratic off-diagonal anti-ME effect, which is expected from the antiferroic order of t_z $(+--+)$ and the $\mathcal{O}_3$ octupoles $(--++)$.

Finally, in Fe_2O_3 [Fig. 2(d)], the induced in-plane magnetic moments perpendicular to the applied electric field have a large linear dependence, with opposite sign on different pairs of Fe atoms. The linear part of the induced moments sums to zero, leading to no net induced moment in the unit cell. This corresponds to an off-diagonal anti-ME effect, following from the antiferroic ordering of t_z, similarly to Cr_2O_3. Interestingly, there is also a substantial quadratic dependence. As the summed (cyan circles) and total (black diagonal crosses) induced moments reveal, this contribution is ferroic and does not sum to zero, instead indicating a net bulk second-order ME response. This is thus the lowest-order ferroic ME response in Fe_2O_3 and follows from the ferroic ordering $(++++)$ of the $\mathcal{O}_3$ octupoles.

Table III summarizes the ME responses discussed above. We note that the proposed anti-ME effect is more ubiquitous than the ferroic ME effect since it follows from less restrictive symmetry requirements. As a consequence, a substantial fraction of magnetic materials is expected to show a local antiferroically ordered ME response.

In this work, we studied the connection between the local ME multipolar order and the local atomic ME response. We discussed as case studies the prototypical ME material Cr_2O_3 and the centrosymmetric material Fe_2O_3. Beyond the well-established linear diagonal ME in Cr_2O_3, we predicted via symmetry and multipole analysis an off-diagonal anti-ME in Cr_2O_3 as well as both diagonal and off-diagonal anti-ME effects in Fe_2O_3 and confirmed our predictions using *ab initio* calculations. Additionally, we found in both materials a non-negligible local second-order ME response, which sums to a net response in Fe_2O_3 and which we rationalized with the presence of magnetic octupoles.

In this way, we showed the strong connection between the orderings of the different ME effects and the underlying ME multipoles and magnetic octupoles. In particular, we identified an antiferroic order of ME multipoles that constitutes a new type of hidden order, adding another example to the growing list of hidden orders in condensed matter physics and highlighting their importance in determining material responses.

Furthermore, our findings allow us to broaden the concept of ME response in ordered materials: To have a local ME response, no global symmetry breaking is required, hence even materials that preserve both inversion and time reversal (the latter composed with a fractional translation), e.g., NiO, allow for a nonzero local ME tensor. The only strict requirement to have any local ME effect is the lack of time reversal among the Wyckoff site symmetries. This means that materials belonging to MSGs of type I (colorless), III, or IV (black-white) allow local ME response; ordered materials of MSG II (gray), instead, do not show any local ME response. If, besides local time-reversal breaking, at least one atomic species sits in a Wyckoff site that is not an inversion center, e.g. Mn_3O_4 [31], then a local *linear* ME response is allowed; otherwise, the lowest-order response is quadratic.

Our calculations show that the local linear anti-ME response is of the same order of magnitude as the local ferro-ME response in similar noncentrosymmetric materials. Thus, the main challenge in measuring an anti-ME response is not the size of the response but rather the antialignment of the induced magnetic moments, producing a vanishing net ME response.

In order to measure and possibly exploit such an anti-ME response, an external electric field varying at the length scale of the unit cell would be desirable, as it would induce a net magnetization. Such electric fields have recently been achieved with twisted bilayer hexagonal boron nitride [46]. A net magnetization could alternatively be achieved by exciting a coherent phonon with the appropriate pattern of polar atomic displacements. Alternatively, the reversed effect, with a uniform magnetic field inducing an alternating polarization in the unit cell, could be detected using second harmonic generation. We hope that our findings motivate further experimental investigations to measure such anti-ME effects, as well as theoretical studies to identify promising candidates with effects of larger size.

The authors thank Dr. Michael Fechner, Dr. John Kay Dewhurst, Dr. Sayantika Bhowal, Dr. Sophie Weber, and Max Merkel for useful discussions. N.A.S., X.H.V., and A.U. were supported by the ERC under the European Union's Horizon 2020 research and innovation programme Grant No. 810451 and by the ETH Zürich. Computational resources were provided by ETH Zürich's Euler cluster.

[1] L. Néel, Propriétés magnétiques de l'état métallique et énergie d'interaction entre atomes magnétiques, Ann. Phys. **11**, 232 (1936).

[2] D. F. McMorrow, K. A. McEwen, U. Steigenberger, H. M. Rønnow, and F. Yakhou, X-Ray resonant scattering study of the quadrupolar order in UPd_3, Phys. Rev. Lett. **87**, 057201 (2001).

[3] M. Kimata, N. Sasabe, K. Kurita, Y. Yamasaki, C. Tabata, Y. Yokoyama, Y. Kotani, M. Ikhlas, T. Tomita, K. Amemiya, H. Nojiri, S. Nakatsuji, T. Koretsune, H. Nakao, T. Arima, and T. Nakamura, X-ray study of ferroic octupole order producing anomalous Hall effect, Nat. Commun. **12**, 5582 (2021).

[4] I. E. Dzyaloshinsky, On the magneto-electrical effect in antiferromagnets, Zh. Eksp. Teor. Fiz. **37**, 881 (1959) [Sov. Phys. JETP **10**, 628 (1960)].

[5] D. Halley, N. Najjari, H. Majjad, L. Joly, P. Ohresser, F. Scheurer, C. Ulhaq-Bouillet, S. Berciaud, B. Doudin, and Y. Henry, Size-induced enhanced magnetoelectric effect and multiferroicity in chromium oxide nanoclusters, Nat. Commun. **5**, 3167 (2014).

[6] N. A. Spaldin and M. Fiebig, The Renaissance of magnetoelectric multiferroics, Science **309**, 391 (2005).

[7] Y. Shiratsuchi, T. V. A. Nguyen, and R. Nakatani, Magnetoelectric control of antiferromagnetic domain of Cr_2O_3 thin film toward spintronic application, J. Magn. Soc. Jpn. **42**, 119 (2018).

[8] Y. Kota, H. Imamura, and M. Sasaki, Enhancement of spin correlation in Cr_2O_3 film above Néel temperature induced by forming a junction with Fe_2O_3 layer: First-Principles and Monte-Carlo Study, IEEE Trans. Magn. **50**, 1 (2014).

[9] M. Fiebig, Revival of the magnetoelectric effect, J. Phys. D: Appl. Phys. **38**, R123 (2005).

[10] L. D. Landau and E. M. Lifshitz, *Electrodynamics of Continuous Media* (Pergamon Press, Oxford, 1960).

[11] Ya. B. Zel'dovich, Electromagnetic interaction with parity violation, Zh. Eksp. Teor. Fiz. **33**, 1531 (1957) [Sov. Phys. JETP **6**, 1184 (1958)].

[12] A. A. Gorbatsevich, Yu. V. Kopaev, and V. V. Tugushev, Anomalous nonlinear effects at phase transitions to ferroelectric and magnetoelectric states, Zh. Eksp. Teor. Fiz. **85**, 1107 (1983) [Sov. Phys. JETP **58**, 643 (1983)].

[13] P. F. de Châtel and A. K. Buin, Toroid dipole moments and hybridization in uranium compounds, Physica B **319**, 193 (2002).

[14] C. Ederer and N. A. Spaldin, Towards a microscopic theory of toroidal moments in bulk periodic crystals, Phys. Rev. B **76**, 214404 (2007).

[15] N. A. Spaldin, M. Fechner, E. Bousquet, A. Balatsky, and L. Nordström, Monopole-based formalism for the diagonal magnetoelectric response, Phys. Rev. B **88**, 094429 (2013).

[16] A. Urru and N. A. Spaldin, Magnetic octupole tensor decomposition and second-order magnetoelectric effect, Ann. Phys. **447**, 168964 (2022).

[17] X. Zhang, Q. Liu, J.-W. Luo, A. J. Freeman, and A. Zunger, Hidden spin polarization in inversion-symmetric bulk crystals, Nat. Phys. **10**, 387 (2014).

[18] L. Yuan, Q. Liu, X. Zhang, J.-W. Luo, S.-S. Li, and A. Zunger, Uncovering and tailoring hidden Rashba spin–orbit splitting in centrosymmetric crystals, Nat. Commun. **10**, 906 (2019).

[19] S. Foner, High-field antiferromagnetic resonance in Cr_2O_3, Phys. Rev. **130**, 183 (1963).

[20] S. Mu, A. L. Wysocki, and K. D. Belashchenko, Effect of substitutional doping on the Néel temperature of Cr_2O_3, Phys. Rev. B **87**, 054435 (2013).

[21] F. J. Morin, Electrical properties of α-Fe_2O_3 and α-Fe_2O_3 containing titanium, Phys. Rev. **83**, 1005 (1951).

[22] I. Dzyaloshinsky, A thermodynamic theory of "weak" ferromagnetism of antiferromagnetics, J. Phys. Chem. Solids **4**, 241 (1958).

[23] At 263 K Fe_2O_3 undergoes the Morin transition to the weakly ferromagnetic phase (until the Néel temperature of 960 K), with the moments lying in the plane perpendicular to the easy axis of the low temperature phase.

[24] R. Hornreich and S. Shtrikman, Statistical mechanics and origin of the magnetoelectric effect in Cr_2O_3, Phys. Rev. **161**, 506 (1967).

[25] P. J. Brown, J. B. Forsyth, and F. Tasset, A study of magnetoelectric domain formation in Cr_2O_3, J. Phys.: Condens. Matter **10**, 663 (1998).

[26] Z. Latacz, Magnetoelectric effect of Cr_2O_3, Acta Phys. Pol. A **97**, 733 (2000).

[27] M. Ye and D. Vanderbilt, Dynamical magnetic charges and linear magnetoelectricity, Phys. Rev. B **89**, 064301 (2014).

[28] T. Kosub, M. Kopte, R. Hühne, P. Appel, B. Shields, P. Maletinsky, R. Hübner, M. O. Liedke, J. Fassbender, O. G. Schmidt, and D. Makarov, Purely antiferromagnetic magnetoelectric random access memory, Nat. Commun. **8**, 13985 (2017).

[29] D. N. Astrov, Magnetoelectric effect in chromium oxide, Zh. Eksp. Teor. Fiz. **40**, 1035 (1961) [Sov. Phys. JETP **13**, 729 (1961)].

[30] L. Šmejkal, J. Sinova, and T. Jungwirth, Emerging research landscape of altermagnetism, Phys. Rev. X **12**, 040501 (2022).

[31] L.-D. Yuan, Z. Wang, J.-W. Luo, and A. Zunger, Prediction of low-z collinear and noncollinear antiferromagnetic compounds having momentum-dependent spin splitting even without spin-orbit coupling, Phys. Rev. Mater. **5**, 014409 (2021).

[32] The relevant input files and data of our ab initio calculations are openly available on the Materials Cloud Archive at http://doi.org/10.24435/materialscloud:x7-6w.

[33] J. Íñiguez, First-principles approach to lattice-mediated magnetoelectric effects, Phys. Rev. Lett. **101**, 117201 (2008).

[34] See Supplemental Material at http://link.aps.org/supplemental/10.1103/PhysRevResearch.5.L042018 for the details regarding the symmetry analysis, the method used to calculate the magnetoelectric response and the parameters that were used for our density functional theory calculations, as well as convergence tests of the canted moment calculations.

[35] J. P. Perdew and A. Zunger, Self-interaction correction to density-functional approximations for many-electron systems, Phys. Rev. B **23**, 5048 (1981).

[36] A. I. Liechtenstein, V. I. Anisimov, and J. Zaanen, Density-functional theory and strong interactions: Orbital ordering in Mott-Hubbard insulators, Phys. Rev. B **52**, R5467 (1995).

[37] G. Kresse and J. Furthmüller, Efficient iterative schemes for ab initio total-energy calculations using a plane-wave basis set, Phys. Rev. B **54**, 11169 (1996).

[38] G. Kresse and J. Furthmüller, Efficiency of ab-initio total energy calculations for metals and semiconductors using a plane-wave basis set, Comput. Mater. Sci. **6**, 15 (1996).

[39] J. K. Dewhurst *et al.*, The Elk code: An all-electron full-potential linearised augmented-plane wave (LAPW) code [https://elk.sourceforge.io/] (2020).

[40] A. Togo and I. Tanaka, First principles phonon calculations in materials science, Scr. Mater. **108**, 1 (2015).

[41] A. Togo, First-principles phonon calculations with phonopy and phono3py, J. Phys. Soc. Jpn. **92**, 012001 (2023).

[42] F. Bultmark, F. Cricchio, O. Grånäs, and L. Nordström, Multipole decomposition of LDA+U energy and its application to actinide compounds, Phys. Rev. B **80**, 035121 (2009).

[43] Note the different choice of cartesian axis with respect to Ref. [16].

[44] The linear out-of-plane response to an in-plane applied electric field is zero, so we do not consider it here.

[45] A. Malashevich, S. Coh, I. Souza, and D. Vanderbilt, Full magnetoelectric response of Cr_2O_3 from first principles, Phys. Rev. B **86**, 094430 (2012).

[46] C. R. Woods, P. Ares, H. Nevison-Andrews, M. J. Holwill, R. Fabregas, F. Guinea, A. K. Geim, K. S. Novoselov, N. R. Walet, and L. Fumagalli, Charge-polarized interfacial superlattices in marginally twisted hexagonal boron nitride, Nat. Commun. **12**, 347 (2021).